



HAL
open science

Influence of crystal orientation and annealing on the oxygen diffusion and surface exchange of $\text{La}_2\text{NiO}_{4+d}$

Mónica Burriel, Helena Téllez, Richard J. Chater, Rémi Castaing, Philippe Veber, Mustapha Zaghrioui, Tatsumi Ishihara, John A. Kilner, Jean-Marc. Bassat

► **To cite this version:**

Mónica Burriel, Helena Téllez, Richard J. Chater, Rémi Castaing, Philippe Veber, et al.. Influence of crystal orientation and annealing on the oxygen diffusion and surface exchange of $\text{La}_2\text{NiO}_{4+d}$. *Journal of Physical Chemistry C*, 2016, 120 (32), pp.17927-17938. 10.1021/acs.jpcc.6b05666 . hal-01377151

HAL Id: hal-01377151

<https://hal.science/hal-01377151>

Submitted on 25 Feb 2021

HAL is a multi-disciplinary open access archive for the deposit and dissemination of scientific research documents, whether they are published or not. The documents may come from teaching and research institutions in France or abroad, or from public or private research centers.

L'archive ouverte pluridisciplinaire **HAL**, est destinée au dépôt et à la diffusion de documents scientifiques de niveau recherche, publiés ou non, émanant des établissements d'enseignement et de recherche français ou étrangers, des laboratoires publics ou privés.

Influence of orientation and annealing on the oxygen diffusion and surface exchange of $\text{La}_2\text{NiO}_{4+\delta}$

Mónica Burriel^{†,‡}, Helena Téllez[§], Richard J. Chater[†], Rémi Castaing^{†,1}, Philippe Veber¹,
Mustapha Zaghrioui[⊥], Tatsumi Ishihara[§], John A. Kilner^{†,§} and Jean-Marc Bassat¹*

[†] Department of Materials, Imperial College London, Exhibition Road, London, SW7 2AZ, UK

[‡] Univ. Grenoble Alpes, CNRS, LMGP, F-38000 Grenoble, France

[§] WPI-I2CNER, Kyushu University, Nishi-ku, Fukuoka, Japan, 819-0395

¹ CNRS, Univ. Bordeaux, ICMCB, 87 Av. Dr Schweitzer, F-33608 Pessac, France

[⊥] GREMAN, UMR 7347 CNRS, Université François Rabelais de Tours, IUT de Blois 15 rue de la Chocolaterie 41 000 Blois, France

ABSTRACT

$\text{La}_2\text{NiO}_{4+\delta}$ is a mixed ionic-electronic conducting material with the 2D K_2NiF_4 -type structure and with a large interest as a potential intermediate temperature solid oxide fuel cell (IT-SOFC) cathode. The oxygen diffusion along the ab plane exhibiting the highest oxygen ionic conductivity governs the behaviour of the bulk materials in this family of oxides. The oxygen surface exchange processes, however, are not well understood and large differences in surface exchange coefficient (k^*) values can be found in the literature for this and other cathode materials. The Isotopic Exchange Depth Profiling (IEDP) technique was used in combination with Low Energy Ion Scattering (LEIS) measurements on two sets of $\text{La}_2\text{NiO}_{4+\delta}$ single crystals with precisely cut crystal faces but different thermal history. For each set of single crystals the oxygen diffusion and surface exchange coefficient were evaluated for 2 different orientations in the temperature range of 450-600 °C. The differences in k^* have been correlated with differences in surface chemistry: surface termination, near-surface rearrangement and presence of extrinsic impurities. Finally, the predominant La- termination at the immediate outer surface is evidenced, confirming recent results in other of Ruddlesden-Popper (RP) phases with mixed ionic-electronic conducting properties.

1. INTRODUCTION

The first members of the Ruddlesden-Popper (RP) series ($A_{n+1}Ni_nO_{3n+1}$ with $n=1$) with nickel as transition metal element are promising materials for the next generation of intermediate temperature ($500 < T \text{ (}^\circ\text{C)} < 700$) solid-oxide fuel cell (SOFC) cathodes¹⁻⁷. This type of $Ln_2NiO_{4+\delta}$ nickelates, with $Ln = La, Nd$ or Pr , possess satisfactory electronic conductivity together with good catalytic, electrochemical and thermo-mechanical properties in the temperature range of interest. Among them, $Pr_2NiO_{4+\delta}$ has shown the best performance when included in a single SOFC cell⁸. However, the lanthanum compound ($La_2NiO_{4+\delta}$) has been the most extensively studied one of the series, with a large amount of experimental data combined with theoretical models reported in the literature. Its fundamental properties, including physical properties, their correlation to the structural characteristics, the oxygen over-stoichiometry and their dependence with temperature and oxygen partial pressure, have been reported for $La_2NiO_{4+\delta}$ polycrystalline samples^{2,9-12}, for single crystals¹³ as well as for epitaxial thin films¹⁴⁻¹⁶. $La_2NiO_{4+\delta}$ can therefore now be considered as a reference material for fundamental studies.

In order to be able to design novel optimized compositions with improved MIEC (Mixed Ionic Electronic Conducting) properties for SOFC cathodes, it is of high importance to precisely identify the oxygen diffusion mechanisms in these RP oxides, which involve three types of oxygen in a two dimensional lattice, leading to highly anisotropic diffusion properties (2D). A number of theoretical calculations have tried to explain and model the oxygen diffusion mechanisms in these nickelates¹⁷⁻²⁰, formed from alternating NiO_2 and $(LnO)_2$ layers along the c-axis direction. The main difference with simple perovskites (state of the art cathode materials), is that in this $Ln_2NiO_{4+\delta}$ structure if $\delta > 0$ the mobile species are usually oxygen interstitials (and not oxygen vacancies), which can accommodate in the $(LnO)_2$ rock-salt layers. Hence no A-site substitution

is required to achieve oxygen mobility in this structure. In addition, acquiring a better understanding of the oxygen reduction reaction (ORR) mechanisms occurring at the surface is key^{5,21} as, at the intermediate temperatures of interest, the ORR is often the limiting process for the cathode performance and its long-term degradation.

For direct experimental measurements of the diffusivity along different directions in this anisotropic structure, single crystals or thin films with very accurate crystallographic orientation must be used. The data available so far are devoted to the measurement of the oxygen diffusion using ^{18}O as a tracer (obtaining both the bulk oxygen diffusion D^* and the surface exchange coefficient k^*) on single crystals oriented along the ab -plane and c -axis directions¹³, and on high quality epitaxial thin films in the two different directions.¹⁴ While the D_{ab}^* and k_{ab}^* values for thin films are close to those measured for single crystals for the ab plane, the corresponding values measured along the c -direction are significantly lower (two to three orders of magnitude)¹⁴. As the results obtained on both sets of samples did not concern exactly the same temperature range (i.e. roughly above and below 500 °C for the single crystals and thin films, respectively), a possible transition between two different dominating mechanisms at different temperatures could also be anticipated. In addition, recent measurements performed between 450 to 700 °C on high quality $\text{Pr}_2\text{NiO}_{4+\delta}$ and $\text{Nd}_2\text{NiO}_{4+\delta}$ single crystals²² confirmed the very large anisotropy between the 2 crystallographic directions (2-3 orders of magnitude). In order to confirm the validity of the previous single crystal data for $\text{La}_2\text{NiO}_{4+\delta}$ and compare differences between different sets of samples, additional data for the low temperature range ($T < 600$ °C) have been performed.

As shown by Ananyev et al²³ for $\text{La}_2\text{NiO}_{4+\delta}$ a relatively large scatter is observed in the literature both for the oxygen diffusion and surface exchange coefficients, as well as for their activation energies. These values vary for different types of samples (single crystals, thin films or

polycrystalline samples), depend on their surface orientation, but also on measuring technique and laboratory of measurement. The source of the discrepancies is not clear, and is generally attributed to different synthesis approaches, surface preparation techniques and differences in microstructure. However up to now the effect of factors which could be key, such as surface cation rearrangement and surface contaminants, have not been taken into account nor have been systematically evaluated. As for the oxygen reduction reaction (ORR), from the impedance spectra analysis Hildenbrand *et al.*²⁴ presented a global model based on an oxygen exchange mechanism in which the surface diffusion of charged oxygen species and the charge transfer with oxygen lattice incorporation would be the two major steps. On the other hand, using the oxygen isotope exchange with the gas phase equilibration technique, Ananyev *et al.*²³ concluded that a two-step model is not valid and propose a three step model, in which the dissociative adsorption would be the rate-determining step. However the k^* values they measured are considerably smaller than those reported for other polycrystal samples, with a larger activation energy. Although they reported the presence of silicon as a surface impurity, its possible relationship with the low k^* values was not discussed in their work.

On the other hand, recent surface chemistry measurements carried out by Low Energy Ion Scattering (LEIS) on the (110) and (001) faces of cleaved $\text{La}_{1.67}\text{Sr}_{0.33}\text{NiO}_{4+\delta}$ single crystals²⁵, on $(\text{La,Sr})_2\text{CoO}_{4+\delta}$ ²⁶ and $\text{La}_{n+1}\text{Ni}_n\text{O}_{3n+1}$ ($n = 1, 2$ and 3)²⁷ epitaxial thin films and on $\text{La}_2\text{NiO}_{4+\delta}$ ²⁸ and $\text{Pr}_{2-x}\text{La}_x\text{NiO}_{4+\delta}$ ²⁹ polycrystalline samples have evidenced that after treatments at high temperatures the surfaces of these RP materials are always dominated by the A-site cations (La, Pr or Sr) of these $\text{A}_{n+1}\text{B}_n\text{O}_{3n+1}$ structures. This predominant surface structure implies that the transition metals (B-site cations), usually invoked as the active sites for the interaction with the gaseous oxygen species, are hidden below the first atomic surface layer(s) and thus their presence at the outermost

surface does not seem to directly control the catalytic activity of these materials^{25,28}. Furthermore, for a number of different electrodes materials³⁰⁻³² it has been recently proved surface segregation takes place in a very short time even at low temperatures (e.g. 15 minutes at 400 °C), giving rise to structural rearrangements. The recent simulation work carried out by Wu et al.³³ has provided some plausible answers to the open question of *why Ni is absent from the surface of La₂NiO_{4+δ}*. The authors found that the decomposition of La₂NiO_{4+δ} to produce La₂O₃ and higher order RP phases is thermodynamically favorable and would leading to a La-terminated and Ni deficient surface.

Hence, the main focus of the present study is to acquire a better understanding of the oxygen exchange processes occurring at the surface of La₂NiO_{4+δ} and relating, for the first time, the catalytic activity of these materials with the surface chemistry and surface reconstruction and poisoning during the high temperature treatments. To this end, Low Energy Ion Scattering (LEIS), a technique which consists in measuring the energy distribution of the backscattered ions (from a low-energy noble gas ion beam) after the collision with the surface³⁴⁻³⁶, will be used to obtain information about the elemental composition of the very first atomic layer and of the near-surface region.

2. EXPERIMENTAL METHODS

2.1 Crystal growth

Single crystals of La₂NiO_{4+δ} were synthesized using the floating zone (FZ) method in an image mirror furnace (Cyberstar) equipped with two 1000 W halogen lamps.

Firstly, polycrystalline powder of La₂NiO_{4+δ} was prepared using a modified citrate method. Citric acid, acrylamide and N,N-bis acrylamide were added to a stoichiometric mixture of La(NO₃)₃ and Ni(NO₃)₂ solutions (La:Ni=2:1). The mixture was heated up to 80 °C to form a gel.

The former was decomposed at 650 °C in air leading to homogeneous and reactive powder, then subsequently annealed at 1000 °C in air to obtain pure $\text{La}_2\text{NiO}_{4+\delta}$ phase. The obtained powder was thereafter compacted to prepare feed rods of 6 mm in diameter and 100 mm in length. Dense feed rods were obtained under isostatic pressure of 300 MPa, then subsequent sintered at 1300 °C for 12 hours in air.

The crystal growth was performed in air using an existent $\text{La}_2\text{NiO}_{4+\delta}$ single crystal as seed and the growth rate was fixed at 3 mm/h. During the growth process, the seed and the feed were counter-rotated at 30 rpm in order to obtain a homogeneous molten zone.

A single crystalline rod of about 5 mm in diameter and 60 mm in length was obtained from the growth. Its crystallinity was checked by Laue X-ray diffraction (XRD). The cationic composition was checked using Energy Dispersive X-ray analysis (EDX), and the cationic ratio of La over Ni was close to 2 (2.00 ± 0.05). The oxygen content was determined using both Thermo Gravimetric Analysis (TGA) under a reducing atmosphere (flowing 5% H_2 in Ar), and iodometric titration on a powder obtained by crushing a piece of single crystal. For TGA analyses, about 100 mg of powder were heated up to 900 °C under Ar/ H_2 5% flux using a heating rate of 2°C/min. The iodometric titration procedure was as follows: about 50 mg of powder was dissolved in a mixture of HBr acid and KI under nitrogen flow. Note that all solutions used during the titration had previously undergone de-oxygenation. The iodine formed by the reduction of Ni^{3+} to Ni^{2+} was then titrated by a thiosulfate solution. The titration was performed using an automated potentiometric titration system (Titroline easy). The oxygen content was thus determined from the total weight loss and the equivalence volume of thiosulfate for TGA analyses and iodometric titration, respectively. The oxygen excess was estimated to be $\delta=0.11\pm 0.01$, a result which is in agreement with the tetragonal structure³⁷ (space group I4/mmm) and cell parameters ($a = 3.87 \text{ \AA}$ and $c =$

12.63 Å) deduced from the powder XRD pattern obtained from a crushed single crystal (

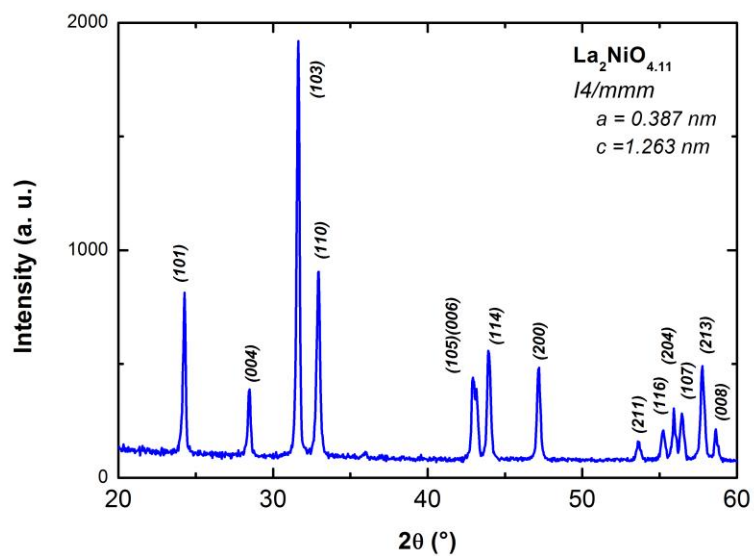


Figure 1).

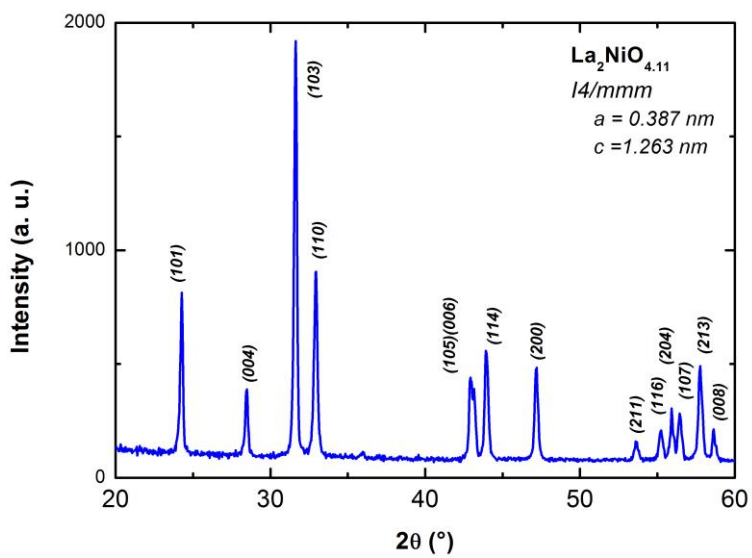


Figure 1 XRD diffraction pattern recorded from a crushed $\text{La}_2\text{NiO}_{4+\delta}$ single crystal

2.2 Crystal orientation

Single crystals fixed on a HUBER 1006 goniometer head were orientated along [100], [010] and [001] crystallographic axes using Laue backscattering method. A 5203.10 HUBER 2-circle segment rotation device was also used to correct the crystal misalignment during the orientation process. The diffraction patterns were collected on KODAK photographic films after a 3-hour stationary crystal irradiation with polychromatic X-ray Bremsstrahlung emitted by a copper anode bombarded by an electron beam (40 mA; 40 kV). Experimental patterns were then indexed with OrientExpress software³⁸ allowing us to orientate crystals with an accuracy of 0.01°.

The cutting of the crystals was performed with a diamond wire saw ESCIL equipped with a 2 circles Micro-check orientation system on which the HUBER goniometer head can be positioned. An accuracy of less than 1° can be reached between the mechanical cut plane and the desired crystallographic one.

Finally, after a polishing of all the faces (down to 250 nm diamond as standard, although in some cases due to size limitations only a lighter polishing was possible), the orientations of the cut faces were accurately checked by the Laue diffraction method using a silicon single crystal as a reference. For this reference crystal we considered a misalignment between the (511) crystal face and its mechanical plane less than 0.01°. This allowed both the positioning and the determination of crystallographic directions of the nickelate crystal as-cut faces perpendicular to the X-rays beam with an absolute accuracy being less than 1° along the 2-circle-segment axis.

2.3 Oxygen isotopic exchange

The oxygen diffusivity (D^*) and the surface exchange coefficient (k^*) of the $\text{La}_2\text{NiO}_{4+\delta}$ single crystals were measured for the low temperature range ($450\text{ °C} < T < 600\text{ °C}$) by the Isotopic Exchange Depth Profile (IEDP) technique, procedure which is described in detail elsewhere^{39,40}. Prior to each exchange, a pre-annealing step was performed, which consisted in equilibrating the

sample at the temperature of interest (same temperature as the subsequent exchange) in dry natural ^{16}O oxygen (99.9% purity with natural abundances for (all) the oxygen isotopes) at 200 mbar. The time used for the pre-anneal step in natural oxygen was always much longer (at least five times) than the exchange time. Then the sample was exchanged in an ^{18}O enriched gas at the same oxygen partial pressure and for a controlled length of time. In order to limit the oxygen stoichiometry change during the heating and cooling ramps, a tubular furnace was rapidly rolled on to set the sample to the annealing temperature and later rolled off to rapidly cool it down. The isotopic oxygen fraction of the ^{18}O enriched gas (0.939 isotopic fraction for set A and 0.260 for set B) was measured by SIMS from the composition of an oxide layer formed on a silicon substrate during an oxidation in the ^{18}O enriched gas at high temperature (1050 °C).

Table 1 Heat pre-treatment sequence (including heat treatment and pre-anneal step in natural oxygen) and ^{18}O exchange exchanges times for each of the $\text{La}_2\text{NiO}_{4+\delta}$ single crystal samples.

		Set A			Set B		
Sample		A_450	A_520	A_600	B_450	B_520	B_600
Dimensions (mm ²) <i>a x b</i>		2.50x1.38	2.15x2.49	1.00x1.00	4.50x1.76	4.60x1.85	4.60x1.85
<i>c</i> (mm)		3.78	2.83	2.25	1.26	2.09	2.09
Exchange temperature (°C)		456	520	595	447	518	594
Heat treatments	Temp. (°C) / Time (h)	None	None	None	341°C/18.8h + 845°C/69.4h	429°C/18.2h + 845°C/69.4h	429°C/18.2h + 845°C/69.4h + 518°C/17.1h + 845°C/72.7h
Pre-anneal in natural oxygen	Time (h)	5	5	5	21.4	17.1	16.6
^{18}O Exchange	Time (s)	3613	2939	2230	2053	1878	909

Two different sets of single crystals have been used for the measurements. With the aim of limiting potential surface segregation processes, the single crystals corresponding to the first set of samples (set A) were exchanged in a gas atmosphere enriched in ^{18}O isotope at 456, 520 and 595 °C after a single short pre-annealing step at the same temperature for 5 h. On the other hand, the second set of samples (set B) were exchanged at similar temperatures (447, 518 and 594 °C) but had a different thermal history, as each sample from this set was used for several exchange experiments. For set B, between each exchange experiment, in order to re-equilibrate the sample to its natural oxygen content, long re-anneal steps were performed at a temperature of approximately 845 °C in natural oxygen (99.999% purity) at 200 mbar. The conditions (gas atmosphere, temperature and time) of each exchange together with the heat treatments sequence (temperature and time) performed to each sample prior to the exchange are detailed in Table 1.

The oxygen diffusion profiles were measured by Secondary Ion Mass Spectrometry (SIMS). The exchange times at each temperature were selected by estimating diffusion length in both directions (from the D^* values for $\text{La}_2\text{NiO}_{4+\delta}$ thin films¹⁴) to be adequate for the SIMS measurement technique used. For a given exchange time, due to the anisotropy of these nickelates, a much shorter diffusion length is expected for the c -axis (see Figure 2) compared to the ab plane.

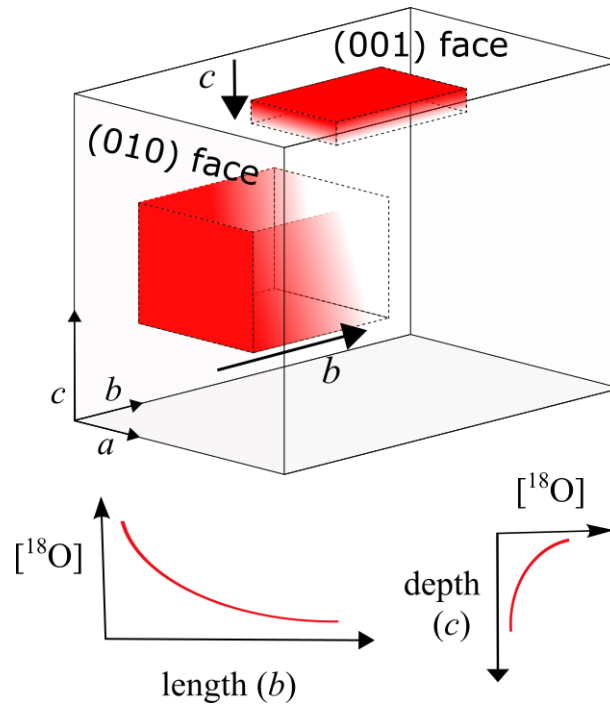


Figure 2 Sketch of the oriented crystals used for the oxygen diffusion measurements along and perpendicular to the c -axis including schematics for the relative ^{18}O diffusion profiles.

2.4 Secondary Ion Mass Spectrometry measurements

The SIMS measurements for samples from set A were determined using a FEI FIB200 ion microscope with a quadrupole-based secondary ion mass spectrometry (SIMS) detector and sputter-etching using a 30 keV Ga⁺ ion beam at 3 nA current.

The diffusion profiles along the *c*-axis were measured on a Focused Ion Beam (FIB) milled and FIB polished ramp surface. The ramp was positioned in approximately the centre of the sample on the top *ab* plane surface and the polished surface of the ramp was approximately at 10° of slope to this *ab* plane surface (9-15°, depending on the sample). The area of the ramps was approximately of 120 μm x 105 μm. Oxygen negative secondary ion mass images were obtained from the ramp surface in order to map the ¹⁸O isotopic fraction down the ramp. A background SIMS map at mass 18.6 amu was also recorded to subtract the non-zero background with the instrument conditions for recording SIMS images. The ramp was also measured in the optical microscope-based white-light interferometer (Zygo Corp, USA NewView200) in order to determine an estimated depth scale. This result also enabled the position of the start of the ramp to be determined and thus the origin of the depth scale. A polished sample of (La,Sr)MnO₃ oxide which had not been exchanged was also analysed in the same SIMS session with the same measurement conditions in order to determine the lower limit of detection of ¹⁸O isotopic fraction.

For the oxygen diffusion along the *ab* plane, in which the diffusion lengths were expected to be much longer, measurements were taken from a FIB ion milled and polished face perpendicular to the *c*-axis, parallel to the original top surface, making sure that it is deep enough to reach a background value of *c*-axis diffusion (see Figure 3). The measured surfaces were at approximately 28, 23 and 70 μm below the top surface for samples A_450, A_520 and A_600, respectively. The oxygen negative SIMS spectra were measured from a series of sputter-etched craters (rectangular

50 μm x 2 μm and approx. 1 μm deep) oriented in the b direction along the polished surface and using a 3 nA 30 keV Ga^+ ion beam. The depth scale for the measurement craters was established using optical microscopy (Zygo). Although for simplicity we will refer to the b -direction, it should be pointed out that as we refer to a tetragonal structure, the a and b directions are equivalent. Finally, as can be observed in Figure 3, one more crater was measured at the top surface to obtain the exact ^{18}O isotopic fraction for length=0.

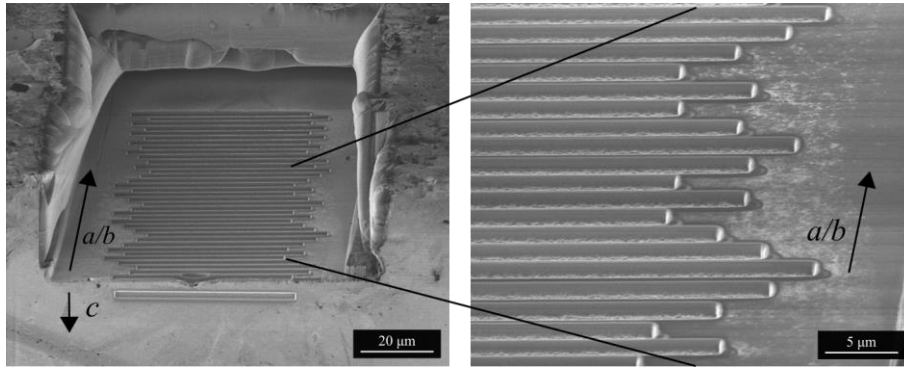


Figure 3 FIB secondary electron images of the c -axis orthogonal polished surface (112 μm x 68 μm) used for the ab plane diffusion measurements for sample A_450. The image was taken at an oblique angle (40°), so that the sputtered craters along the b direction together with the surface crater are clearly observable.

The exchanged single crystals from set B were measured by time-of-flight SIMS on a TOF.SIMS 5 instrument (IONTOF GmbH, Münster, Germany) equipped with a pulsed bismuth liquid metal ion gun incident at 45° operated in the burst alignment mode (7 or 8 peaks) and the Cs^+ beam (~ 200 nA, 2 kV at 45° incidence) for sputtering. The depth profiling mode for oxygen isotopes described in detail by De Souza *et al.* ⁴⁰, was used for the c -axis diffusion measurement, as it allows determining species distribution in depth from the outer surface of the material using a high depth resolution. The depth profile was measured in a face perpendicular to the c -axis, in

the center of the sample to ensure no contribution from the *ab*-plane diffusion (see Figure 2). For the measurement of the oxygen diffusion along the *ab* plane, a crater was sputtered with the Cs⁺ beam (2 kV) at the edge of the crystal on a face perpendicular to the *c* axis. In this configuration the SIMS measurements were recorded from the center of the receding base of the sputtered crater as a series of images⁴⁰.

After the SIMS measurement, the depth of the sputter-etched craters (*c*-axis profiles) was measured using the optical microscope-based interferometer (Zygo Corp. NewView 200).

2.5 Low Energy Ion Scattering (LEIS) measurements

The outermost surface composition of the samples was measured with monolayer atomic resolution by Low Energy Ion Scattering (LEIS) (Qtac¹⁰⁰, IonTOF GmbH, Germany). Prior to the analyses, the samples were cleaned *ex-situ* in an ultrasonic bath (10 min in acetone/ 10 min in ethanol / 10 min in de-ionised water) and dried in air. Since LEIS is very surface-sensitive, the sample surface was also cleaned *in-situ* prior to the analysis in order to remove the organic contaminants remaining from the brief exposure to the atmosphere. This cleaning process was performed by oxidation using reactive atomic oxygen flux (O) that removes the hydrocarbons on the surface (i.e. the O atoms react with the adventitious hydrocarbons forming volatile species that are pumped out of the preparation chamber). The pressure in the preparation chamber during the cleaning process is about $\sim 5 \times 10^{-5}$ mbar due to the flux of the reactive atomic oxygen. The sample was then transferred from this preparation chamber into the main analysis chamber (base pressure 1×10^{-10} mbar) without further air exposure. The effectiveness of the cleaning was checked by analysing the surface with a 3 keV He⁺ beam to check the presence of a C peak (theoretical position of about 846 eV). The He⁺ ion dose used during these analyses was very low in order to avoid surface sputtering that would remove the organic contamination and could be misinterpreted as an

effective cleaning by oxidation with atomic oxygen. Therefore, each analysis was acquired using less than 4×10^{13} ions/cm² per analysis, and the total ion dose for the sequential analyses on the same area was less than 2×10^{14} ions/cm² for the total cleaning check. Note that, for those cases where there are carbonates on the surface, the cleaning procedure would be ineffective to remove these species and a C peak will be still detectable in the He⁺ spectrum. A second indicator of the surface cleaning is given by the surface peaks corresponding to other heavier cations (e.g. La), which shows much higher yields than the C atoms. Therefore, the oxidation was repeated until identical surface spectra were obtained for two consecutive He⁺ analyses, showing the same La surface coverage (peak areas).

The LEIS surface analysis was performed using a 3 keV He⁺ ion beam at normal incidence to the surface over an area of 1 mm². The ion fluence during the analysis was kept below 5×10^{13} ions/cm² in order to avoid a significant surface damage. For depth profiling, the dual beam mode was used combining analysis steps with a 3 keV He⁺ beam followed by sputter steps using a 500 eV Ar⁺ beam at 59° incidence angle to erode the material. The mean projected range for the sputter ions under these conditions is estimated to be 1.0 nm⁴¹. The ion fluence per sputtering step was about 1×10^{15} ions/cm², in order to remove the more extended atomic mixing caused by the primary ion beam (due to the energy and angle of sputtering beam, the mixing due to sputtering is much lower than that produced during the analysis).

3. RESULTS AND DISCUSSION

3.1 Oxygen diffusion and surface exchange coefficients along the two main crystallographic directions

The first aim of present study is to measure both D^* and k^* coefficients in the two main crystallographic directions on $\text{La}_2\text{NiO}_{4+\delta}$ single crystals for the low temperature range ($400 < T < 600$ °C). For this purpose a new device was used for the preparation of single crystal samples with highly precise crystallographic orientations ($< 1^\circ$ for both directions), as described in the Experimental section.

From the ^{16}O and ^{18}O SIMS intensity data acquired, the normalized ^{18}O isotopic fraction $c'(x)$ was calculated as showed in Equation 1:

$$c'(x) = \frac{c^*(x) - c_{bg}^*}{c_g^* - c_{bg}^*} \quad (\text{Equation 1})$$

Where $c^*(x)$ is the ^{18}O isotope fraction obtained by SIMS, i.e. $^{18}\text{O}/(^{18}\text{O}+^{16}\text{O})$, c_{bg}^* is the background isotope fraction and c_g^* is the isotope fraction of the annealing gas. The data were fitted using the solution of the diffusion equation given by Crank⁴² in terms of the dimensionless parameters $x' = \frac{x}{2\sqrt{D^*t}}$ and $h' = \frac{k^*}{D^*}\sqrt{D^*t}$ for diffusion in a semi-infinite medium with surface limitation and constant c_g^* ⁴² (Equation 2):

$$c'(x) = \text{erfc}(x') - \exp(2h'x' + h'^2) \times \text{erfc}(x' + h') \quad (\text{Equation 2})$$

where D^* is the tracer oxygen diffusion coefficient and k^* the tracer surface exchange coefficient.

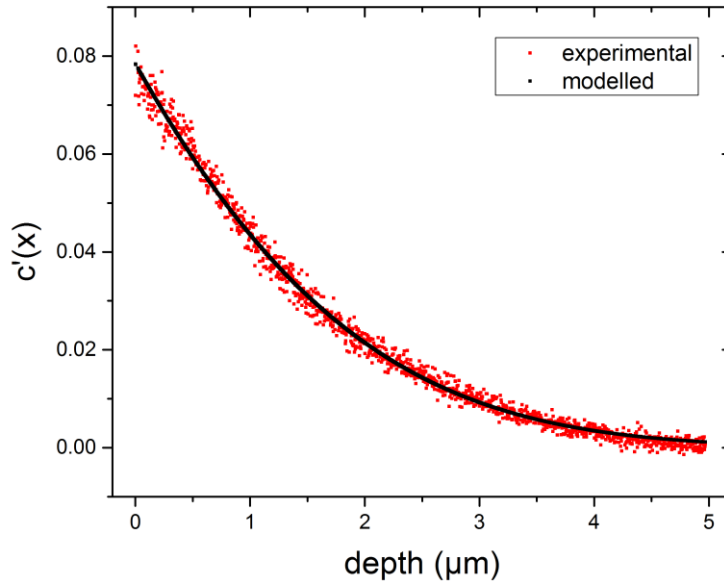


Figure 4 Normalised ^{18}O diffusion profile along the c axis for the single crystal exchanged at $T = 594$ °C for 909 s (set B) and fit to Crank's solution to Fick's second law.

Figure 4 shows an example of a diffusion profile obtained along the c axis for the $\text{La}_2\text{NiO}_{4+\delta}$ single crystal exchanged at $T = 594$ °C (sample B_600). The oxygen diffusivity (D_c^*) and the surface exchange coefficient (k_c^*) values calculated for the best fit are $2.9 \cdot 10^{-11}$ cm^2/s and $1.3 \cdot 10^{-8}$ cm/s , respectively.

The fitted D^* and k^* coefficients in both directions are included in

Table 2 together with the dimensionless parameter h' for all the measured samples (set A and set B) and temperatures. Due to the very large anisotropy in D^* between the 2 crystallographic directions (2-3 orders of magnitude) for $\text{La}_2\text{NiO}_{4+\delta}$, obtaining measurable diffusion profiles for both directions in a single exchange is rather challenging. For low k^* values (in relation to D^*) very low h' values are obtained, which results in very small differences between the surface and

the background ^{18}O levels. Along the ab plane direction (fast diffusion direction) low ^{18}O surface concentrations, only slightly above background, were obtained for the lowest measured temperature (~ 450 °C) for set A ($c'(0) \approx 0.001\text{-}0.002$) and for all temperatures for set B ($c'(0) \approx 0.004\text{-}0.015$). In those cases it was not possible to extract reliable surface exchange and diffusion coefficients from the fits.

Table 2. The oxygen diffusivity (D_{ab}^* and D_c^*), the surface exchange coefficient (k_{ab}^* and k_c^*) values and the dimensionless parameter h' along and perpendicular to the c -axis calculated from the experimental oxygen diffusion profiles.

Temp. (°C)	<i>ab plane</i>			<i>c-axis</i>					
	D_{ab}^* (cm ² /s)	k_{ab}^* (cm/s)	h'	D_c^* (cm ² /s)		k_c^* (cm/s)		h'	
	Set A	Set A	Set A	Set A	Set B	Set A	Set B	Set A	Set B
456/447			<<	$2.8 \cdot 10^{-11}$	$4.0 \cdot 10^{-12}$	$1.6 \cdot 10^{-8}$	$8.0 \cdot 10^{-11}$	0.137	0.002
520/518	$2.0 \cdot 10^{-8}$	$7.0 \cdot 10^{-8}$	0.027	$3.0 \cdot 10^{-11}$	$1.3 \cdot 10^{-11}$	$2.0 \cdot 10^{-7}$	$1.5 \cdot 10^{-9}$	1.58	0.018
595/594	$5.6 \cdot 10^{-8}$	$5.1 \cdot 10^{-7}$	0.101	$3.4 \cdot 10^{-11}$	$2.9 \cdot 10^{-11}$	$3.1 \cdot 10^{-6}$	$1.3 \cdot 10^{-8}$	15.9	0.074

A large anisotropy was measured for the oxygen diffusion, being 3 orders of magnitude larger along the a - b plane than along the c -axis for the measured temperature range (see Figure 5 and Table 2). The D_{ab}^* values ($>10^{-8}$ for $T \geq 520$ °C) are similar (slightly larger) to those previously reported for single crystals¹³ and slightly higher to reported for polycrystalline bulk samples^{2,9,43} but with a similar activation energy. This clearly indicates that the diffusion along the ab plane (D_{ab}^*) governs the behaviour of the bulk material. The D_c^* values obtained for the single crystals with and without heat treatments (sets B and A) are quite similar, although the small activation

energy obtained points to a possible limitation in experimental method (lower limit of about $(2\pm 1) \times 10^{-11} \text{ cm}^2 \text{ s}^{-1}$) and thus the values obtained correspond to the lower bound of the diffusion coefficient along the c -axis. Furthermore, the good agreement with the D_c^* values previously reported for thin films¹⁴ confirm the very large anisotropy between both directions ($\geq 10^3$) and indicates that the D_c^* values had been overestimated in previous single crystal measurements due to previous orientation and cutting limitations¹³.

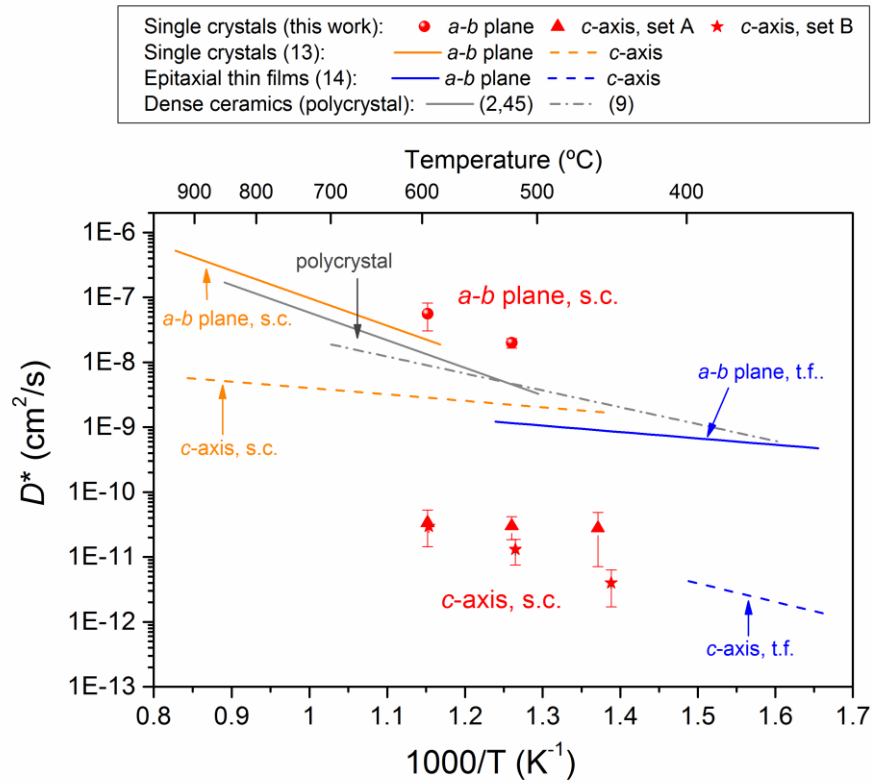


Figure 5 Diffusion coefficients obtained for the $\text{La}_2\text{NiO}_{4+\delta}$ single crystals and comparison to literature data on ceramic pellets^{2,9,43}, single crystals¹³ (s.c.) and thin films¹⁴ (t.f.).

Figure 6 shows the comparison between the D^* coefficients in both directions for all the $\text{La}_2\text{NiO}_{4+\delta}$ measured single crystals (sets A and B) and the literature values for $\text{Pr}_2\text{NiO}_{4+\delta}$ and $\text{Nd}_2\text{NiO}_{4+\delta}$ single crystals. The three lanthanide nickelates (La, Nd and Pr) present similar diffusion

anisotropy and activation energies, being $\text{La}_2\text{NiO}_{4+\delta}$ and $\text{Pr}_2\text{NiO}_{4+\delta}$ the compositions with highest oxygen diffusivity coefficients.

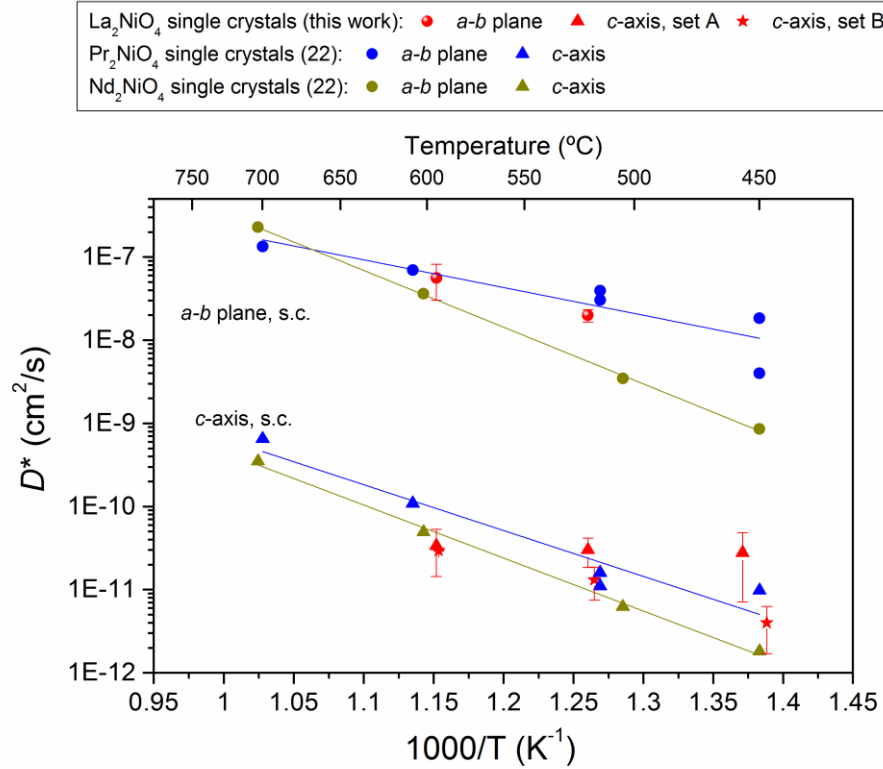


Figure 6 Diffusion coefficients obtained for the $\text{La}_2\text{NiO}_{4+\delta}$ single crystals along and perpendicular to the c -axis crystals and comparison to literature data on $\text{Pr}_2\text{NiO}_{4+\delta}$ and $\text{Nd}_2\text{NiO}_{4+\delta}$ ²²

The fitted k^* coefficients in both directions for all the measured samples (sets A and B) and temperatures and their comparison with literature values for other $\text{La}_2\text{NiO}_{4+\delta}$ samples are included in Figure 7. It can be observed that for set A (samples with a short pre-anneal step) for the measured temperature range the k_{ab}^* and k_c^* values are quite comparable (although slightly larger for the c -axis). As the similarity in surface exchange coefficient for both orientations was unexpected, this motivated an in-depth study of the outer and near-surface chemistry. As will be explained in the next section, the surface chemistry of this type of compounds is dynamic and will depend on the

composition and thermal history of each sample and face, being the surface exchange coefficient differences directly related to these time-dependent chemical differences.

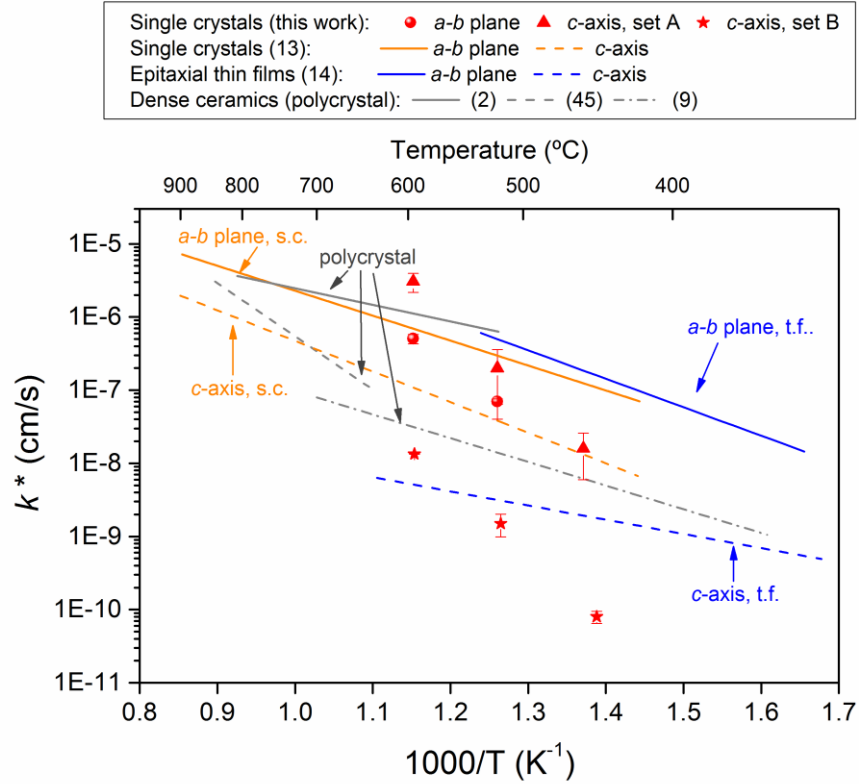


Figure 7 Surface exchange coefficients obtained for the $La_2NiO_{4+\delta}$ single crystals and comparison to literature data on ceramic pellets^{2,9,43}, single crystals¹³ (s.c.) and thin films¹⁴ (t.f.).

Figure 8 shows the comparison between the k^* coefficients in both directions for the $La_2NiO_{4+\delta}$ single crystals measured after a short pre-anneal step (set A) and the literature values for $Pr_2NiO_{4+\delta}$ and $Nd_2NiO_{4+\delta}$ single crystals. It can be observed that both the $a-b$ plane surface exchange coefficients and their activation energy are very similar for the 3 compositions (La, Pr and Nd). However the k_c^* value obtained for the $La_2NiO_{4+\delta}$ single crystals is larger than for the other compounds, and not very different from its k_{ab}^* value.

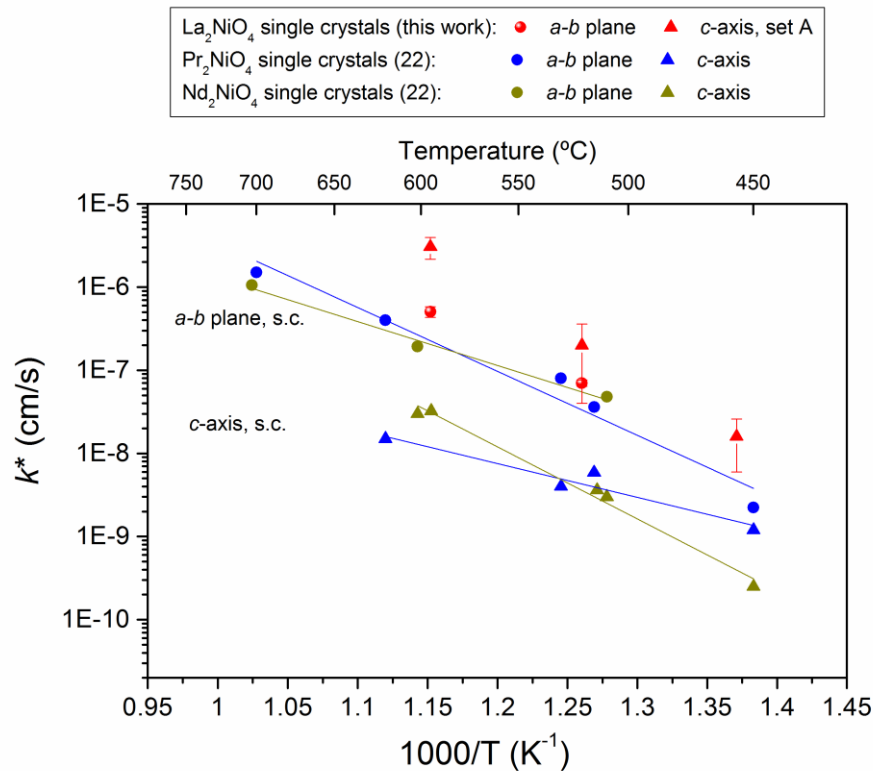


Figure 8 Surface exchange coefficients obtained for the $La_2NiO_{4+\delta}$ single crystals along and perpendicular to the c-axis crystals and comparison to literature data on $Pr_2NiO_{4+\delta}$ and $Nd_2NiO_{4+\delta}$ ²²

LEIS measurements were performed with the aim of understanding the relationship between the surface exchange coefficient values and the composition of the outer and near surface for different faces and for samples submitted to different thermal history. With this aim the single crystal samples A_450 and B_450 exchanged around 450 $^{\circ}C$ were selected. Sample A_450 had only been pre-annealed at 456 $^{\circ}C$ in natural oxygen for 5 h prior to the ^{18}O exchange, while sample B_450 had followed a sequence of anneals including 113.8 h at 845 $^{\circ}C$ (see **Erreur ! Source du renvoi introuvable.**).

3.2 Impact of surface orientation on the surface exchange coefficient

Figure 9.a and 9.b show the outer surface LEIS spectra obtained with a 3 keV He⁺ beam of the (001) and (010) faces of the single crystal from set A after the exchange. The surface composition for both orientations was found to be similar. A very clean surface was measured in both cases, with no contamination peaks detected. Three main elements are present in the outermost surface of the crystals, which correspond to the 3 detected peaks: ¹⁶O, ¹⁸O and La (theoretical peak positions at 1181.7, 1316.2 and 2701.3 eV, respectively). The expected position of the Ni peak (theoretical peak position of 2332.2 eV, for the most abundant isotope) is also marked in the spectra. The lack of a peak in this position reveals that no Ni can be detected at the outermost surface of these crystals, at least to the detection limit of the technique that is estimated to be 15% for Ni using 3 keV He⁺, and thus it can be concluded that both surfaces are LaO-terminated.

The preferential A-site termination at the immediate outer surface of Ruddlesden-Popper (RP) phases containing Ni as the transition metal ion has also been recently observed for La_{1.67}Sr_{0.33}NiO_{4+δ} single crystals²⁵ and for La₂NiO_{4+δ}²⁸ and Pr_{2-x}La_xNiO_{4+δ}²⁹ polycrystalline samples after anneal treatments in air at 450 °C and in pure oxygen at 800 and 1000 °C, respectively. Even after the deposition of La₂NiO_{4+δ} epitaxial thin films by pulsed-laser deposition (PLD) at about 700 °C (*c*-axis oriented), the preferred surface termination determined by LEIS is the LaO-plane, as reported by Wu²⁷. Further evidence of layer re-arrangements leading to AO surface termination in Ruddlesden-Popper (LaO)(LaNiO₃)_n phases has been theoretically predicted and experimentally demonstrated in reference 44. Hence these measurements support the postulation that the general assumption of the B-site cations exposed to the environment controlling the catalytic activity of the materials may be incorrect.

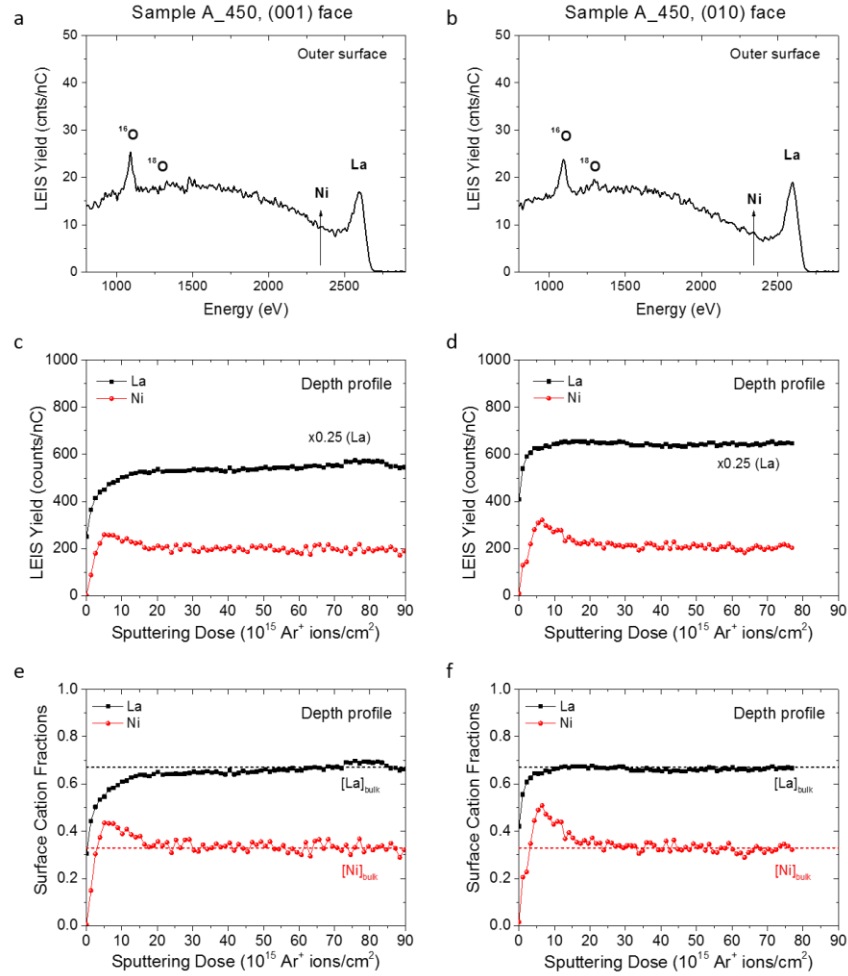


Figure 9. Sample A_450 ($\text{La}_2\text{NiO}_{4+\delta}$ single crystal treated at 450°C): He^+ LEIS spectra for the outer surface measured for (a) the (001) and (b) the (010) faces. LEIS depth profiles on (c) the (001) face (c -axis direction) and (d) the (010) face (ab -plane). The raw intensities for La surface atoms were scaled for clarity. Surface cation fractions normalized to the bulk stoichiometry, as obtained from the LEIS depth profiles, for (e) the (001) face (c -axis direction) and (f) the (010) face (ab -plane).

Depth profiling analysis of the single crystals was performed by alternating the analysis cycle (using the 3 keV He^+ analytical beam) and low-energy sputtering steps (using 500 eV Ar^+ sputtering, with an ion fluence of 10^{15} ions/ cm^2 for each sputtering cycle). The LEIS yield depth

profiles and surface cation fractions obtained for the single crystal treated at 450°C (sample A_450) are shown in Figure 9.c and 9.e for the (001) face (*c*-axis direction) and in Figure 9.d and 9.f for (010) face (*ab*-plane). The fractions were estimated by using the bulk cation intensities as a reference value for the bulk stoichiometry of the $\text{La}_2\text{NiO}_{4+\delta}$ single crystal. For both orientations there is a fast increase of the Ni intensity after removing the first layer of atoms, with a maximum at an ionic fluence of 5×10^{15} ions/cm². After this maximum, the Ni intensity decreases again reaching an intensity plateau after a sputtering fluence of approximately 20×10^{15} ions/cm². The Ni cation fractions (normalized to the bulk stoichiometry) revealed a Ni-enriched subsurface for both faces, reaching values of 0.44 for the (001) face (Figure 9.e) and of 0.51 for the (010) face for sample A_450. This clearly demonstrates that a cation rearrangement has taken place within the $\text{La}_2\text{NiO}_{4+\delta}$ and that the outer surface might have lost its structural anisotropy due to the formation of other phases at the surface and sub-surface. The existence of this Ni-rich near-surface region is in agreement with previous studies performed both on $\text{La}_2\text{NiO}_{4+\delta}$ ceramic samples after high temperature treatments²⁸ and on as-deposited Ruddlesden-Popper $\text{La}_{n+1}\text{Ni}_n\text{O}_{3n+1}$ ($n = 1, 2$ and 3) epitaxial films.²⁷ Gauquelin *et al*⁴⁵ had shown that long-term annealing of $\text{La}_2\text{NiO}_{4+\delta}$ single crystals in air at very high temperatures (1273 K) leads to the formation of nickel-rich Ruddlesden–Popper phases ($n = 2$ and 3) at the single-crystal surfaces. Recent studies on epitaxial $(\text{La,Sr})_2\text{CoO}_{4+\delta}$ RP thin films showing similar B-site enriched regions, revealed that this B-enrichment seems to be related to the formation of additional phases due to the decomposition of the RP phase at the near-surface region²⁶. Furthermore, as previously explained, a recent evaluation of the thermodynamic stability of $\text{La}_2\text{NiO}_{4+\delta}$ ³³ suggests that a partial decomposition of $\text{La}_2\text{NiO}_{4+\delta}$ is thermodynamically favorable and could take place at the surface when exposed to air. The decomposition would lead to a stacking of (La_2O_3) – $(\text{La}_3\text{Ni}_2\text{O}_7$ and/or $\text{La}_4\text{Ni}_3\text{O}_{10})$ – $(\text{La}_2\text{NiO}_4)$, that would be responsible for

the observed Ni-absence and for the Ni:La non-stoichiometry at $\text{La}_2\text{NiO}_{4+\delta}$ surfaces. This explanation is in perfect agreement with our results and would explain the higher Ni cation fraction observed for the sample which had been subject to longer anneal times, as will be shown in the next section.

The similar compositional rearrangement found for both orientations (Figure 9e and 9f) could be at least in part responsible for the lack of anisotropy in the surface exchange coefficients (Figure 7) obtained for these $\text{La}_2\text{NiO}_{4+\delta}$ single crystals (set A). Any sub-surface atomic rearrangement that might affect the near-surface composition could override the expected anisotropy of the oxygen exchange at the surface. Similar findings have also been recently found for $(\text{La,Sr})_2\text{CoO}_{4+\delta}$ epitaxial thin films with RP structure²⁶, which was explained by surface segregation effects that override the effect of the structural anisotropy.

In view of these results, it is evident that the time used for the pre-anneal step (usually recommended at least 10 times longer compared to the exchange itself for the IEDP technique⁴⁶), as well as any other anneal steps carried out, must be taken into consideration when comparing k^* values for different sets of samples. Alteration of the composition due to matrix atom segregation at high and even intermediate temperatures is certainly possible, and these chemical variations should be carefully considered when evaluating the surface exchange of electrochemically active materials.

3.3 Impact of long anneal treatments and impurities on the surface exchange coefficients

A large variation in the k^* coefficients can be observed for different sets of samples when comparing among the different literature values for $\text{La}_2\text{NiO}_{4+\delta}$ (Figure 7). For example a 2-orders of magnitude difference can be observed between the polycrystal samples measured by Boehm et al.² and those measured by Sayers et al.⁹ These results indicate that differences between batches

and the thermal history of the samples can have a larger effect in the surface exchange properties of the material than the crystal orientation.

As for the comparison between both sets of single crystals, despite having shown very similar diffusion coefficients (see Figure 7), a very large difference in the surface exchange is observed between the samples submitted to long heat treatments (set B) and those only submitted to a short pre-anneal (set A). k_c^* decreases more than 2 orders of magnitude after the high temperature treatments. Although it was not possible to extract accurate k_{ab}^* coefficients for set B, this limitation (low C' at the surface) clearly comes from the fact that the k_{ab}^* coefficients are also very low.

Erreur ! Source du renvoi introuvable. a and b show the LEIS surface spectra of the (001) and (010) faces of the single crystal sample B_450 after long exchange and heat treatment, which included a total of 113.8 h at 845 °C. In this case in addition to the ^{16}O , ^{18}O and La peaks, the surface shows the presence of several contaminants, mainly Na for an onset energy (theoretical position) of 1581.2 eV (^{23}Na), Ca or K (2081.1 eV for ^{40}Ca and 2061.5 eV for ^{39}K), Cr (around 2265.2 eV) and Pt or Au (2784.1 eV for ^{195}Pt and 2786.2 eV for ^{197}Au). Although the same contaminants were found for both faces of the single crystal, the intensity of each peak (element) largely depends on the region and face analysed as the contamination over the surface is non-uniform. As the position for ^{40}Ca and ^{39}K peaks and for ^{195}Pt and ^{197}Au peaks are very close, ToF-SIMS measurements were used to check the correct assignment of the peaks, confirming the presence of Ca and Pt as minor outer surface contaminants.

The spatial distribution of the contaminants on the surface can be obtained from the integration images of the LEIS depth profiles, as shown in Figure 11. Although the images were obtained with low resolution in order to avoid damage by focussing the beam onto a small surface spot, some

regions covered by the impurities were clearly observed. In the case of the (001) face of sample B_450, mainly a small region at the edge of the analysed area showed the presence of Na and Ca impurities, while Pt was found over all the analysed surface. Interestingly, the ^{18}O and ^{16}O images showed a positive correlation with the impurities chemical maps. The Pt intensity is low and easily removed after a few sputtering cycles.

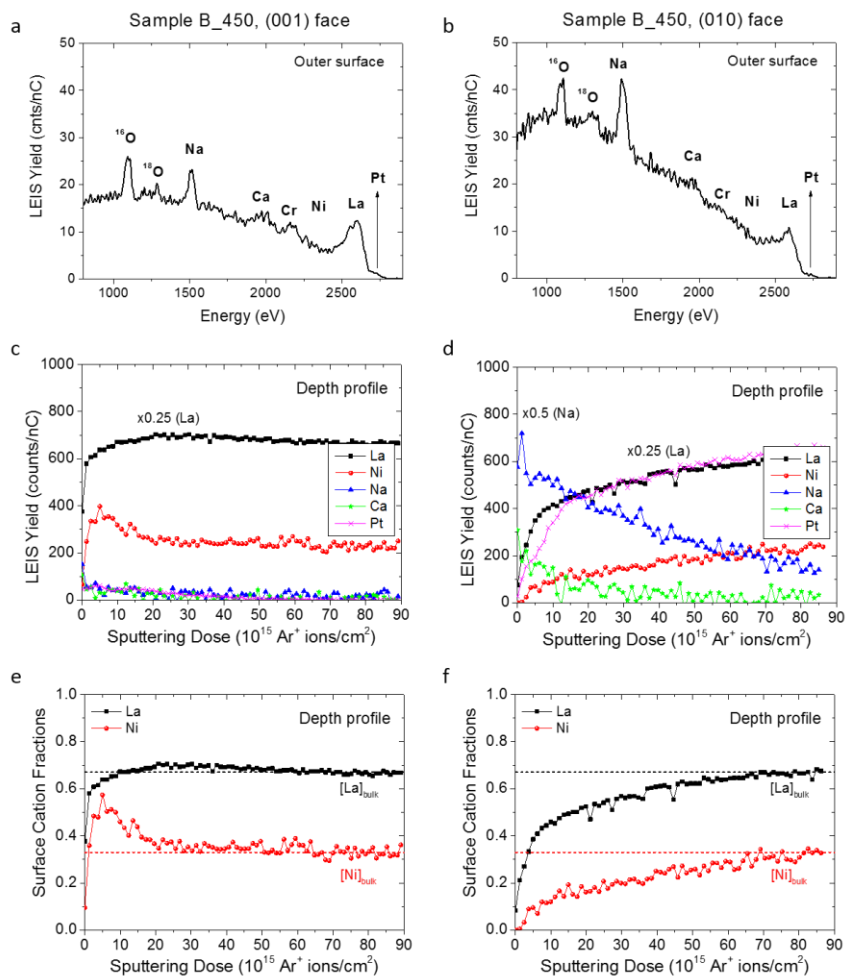


Figure 10 Sample B_450 ($\text{La}_2\text{NiO}_{4+\delta}$ single crystal treated at 450°C): He^+ LEIS spectra for the outer surface measured for (a) the (001) and (b) the (010) faces. LEIS depth profiles on (c) the (001) face (*c*-axis direction) and (d) the (010) face (*ab*-plane). The raw intensities for La surface atoms were scaled for clarity. Surface cation fractions normalized to the bulk stoichiometry, as

obtained from the LEIS depth profiles, for (e) the (001) face (*c*-axis direction) and (f) the (010) face (*ab*-plane).

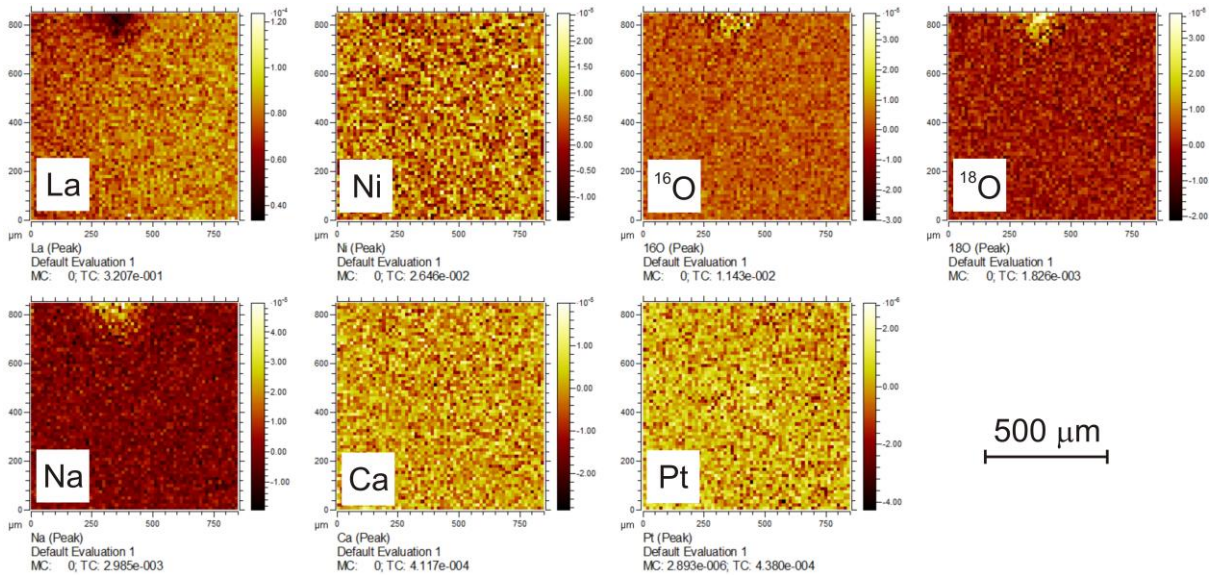


Figure 11 Elemental chemical maps obtained for the constituent elements and impurities after the long heat-treatments (sample B_450) on the (001) face. The images are obtained by integrating the LEIS spectra obtained during the whole depth profiling analysis. The intensity range is indicated below for each individual chemical map.

The LEIS depth profiles on the (001) and (010) faces (*c*-axis direction *ab* plane) obtained for the single crystal treated at 450°C after long heat treatments (sample B_450) are shown in **Erreur ! Source du renvoi introuvable..a** and **Erreur ! Source du renvoi introuvable..b**, respectively. The Na, Ca and Pt impurities present on the (001) face are rapidly removed by the sputtering, all peaks disappearing after a total fluence of 4.0×10^{16} ions/cm². However a larger amount of impurities are present on the (010) face, being the Na and Pt still present after a total fluence of 8.5×10^{16} ions/cm². The exact source of the surface contaminants is yet to be confirmed and a

number of different possibilities are conceivable. Ceramics invariably contain some impurities, which tend to segregate to the grain boundaries and surfaces during heat treatments. Na and Ca are common impurities found in oxide materials, such as yttria stabilized zirconia (YSZ)⁴⁷. The presence of Na could also come from handling the crystals or of the silica tubes used in the experimental setup, while Ca, Cr and Pt could come from cross-contamination with other samples. These elements might have deposited in the internal parts of the experimental setup and could have evaporated at the high re-anneal temperatures in pure oxygen at 845 °C and have re-deposited on the surface of the single crystals. It should be pointed out that to avoid cross-contamination with other samples a single silica exchange tube, thermocouple cover and silica boat (to place the samples) were used for the anneal and exchange experiments of the nickelate single crystals. The observed surface contamination was thus unexpected.

Long-term surface poisoning due to external impurities as well as surface cation segregation processes have implications for the electrochemical performance of SOFCs, leading to the degradation of the cell components⁴⁸. Na, Ca, Cr and Pt are common elements forming part of the SOFC ceramic layers, chromium-containing interconnects and experimental setup elements (thermocouples, wires, electrodes, etc), and can be therefore common impurities in typical electrochemical experiments and devices. Thus the influence of these impurities in the properties of these cathode materials is of great interest of the application of these compounds in real electrochemical devices.

After long heat treatments the surface exchange coefficient measured for the (001) faces was observed to decrease more than 2 orders of magnitude (from $1.60 \cdot 10^{-8}$ and $8.0 \cdot 10^{-11}$ at 450°C from sample A_450 to sample B_450) (see Figure 7) for an estimated surface coverage of impurities of around 27%, while the effect on the (010) faces was such that resulted in an un-measurable

diffusion profile along the *ab* plane (i.e. estimated impurity coverage of about 81%). In order to compare the near-surface composition between samples and faces, Figure 10.e and f show the surface cation fractions as a function of the sputtering fluence for the (001) and (010) faces of sample B_450. It should be mentioned that the sputtering fluence for each set of samples might vary due to the surface roughness differences as the erosion rate might be faster for the rougher surface. For instance, the B_450 samples were subjected to long heat treatments, and hence, the roughness is affected by the annealing step. In addition, the impurities at the outer region of the B_450 samples might also show a different sputtering rate compared to the pristine $\text{La}_2\text{NiO}_{4+\delta}$ surface. Therefore, any comparison between the depth profiles must consider the sputtering rate difference depending on the outer composition and the surface roughness.

As for the in-depth variation of the surface cation fractions obtained by LEIS, for face (001) there is a fast increase of the Ni intensity after removing the first layer of atoms, with a maximum at an ionic fluence of 5×10^{15} ions/cm², followed by a decrease reaching an intensity plateau after a sputtering fluence of approximately 20×10^{15} ions/cm² (Figure 10.e). This in-depth rearrangement of the La and Ni cations is very similar to that observed the uncontaminated sample submitted to short heat treatments (Figure 9.e), although higher Ni cation fractions (up to 0.57) were measured for sample B_450 (after long-time anneals) compared to 0.44 for sample A_450. As for the surface cation fractions for face (010), these are strongly affected by a large amount of surface impurities and reach the stoichiometric values after a sputtering fluence of approximately 85×10^{15} ions/cm².

These results clearly highlight the strong detrimental effect that common impurities have upon the oxygen exchange rate for $\text{La}_2\text{NiO}_{4+\delta}$. A relationship between the surface exchange and cathode performance decrease with the appearance of surface contaminants has been previously been observed by other authors for contaminants such as C, S, Si, Na, Ca and Cr for both electrode and

electrolyte materials^{48,49}. In particular by performing LEIS surface measurements, De Ridder *et al.* showed that bulk impurities, such as SiO₂, CaO and Na₂O, segregate to the outermost surface layer of YSZ until they completely cover it creating an impenetrable barrier for oxygen. This surface exchange reduces to zero for a completely covered surface by reducing the area available for oxygen exchange.

CONCLUSIONS

The oxygen diffusion of high quality La₂NiO_{4+δ} single crystals was measured along 2 perpendicular directions using the IEDP technique. An anisotropy of 3 orders of magnitude was obtained for the measured temperature range (450-600 °C), the diffusivity being larger along the *a-b* plane than along the *c*-axis. From the intrinsic oxygen diffusion and surface exchange values obtained it can be concluded that for the intermediate temperature range of operation (450-600 °C) La₂NiO_{4+δ} and Pr₂NiO_{4+δ} are the most promising cathode materials within the family, as they possess the highest D^* and similar k^* values.

The oxygen diffusion coefficient is not affected by the thermal history of the sample. However the surface exchange is strongly related to the thermal history of the sample and very largely affected by the presence of common impurities and surface rearrangement processes, which explains the large scatter in k^* values commonly found in the literature for a given materials composition. It has been proved that even in the absence of external impurities, the surface of La₂NiO_{4+δ} tends to decompose and reconstruct into other RP phases. Similar k_c^* and k_{ab}^* values were obtained for the 2 orientations, which is thought to be related to similar cationic surface rearrangement for different surface orientation. The lack of anisotropy in the surface exchange

values for both surfaces measured in this work is most likely related to the surface segregation process overriding the intrinsic anisotropy of the material.

In addition, the surface exchange coefficient k_c^* has been shown to decrease more than 2 orders of magnitude after long temperature treatments which seems to be related to the existence of surface impurities. These elements can come directly from the gas surrounding the surface or from traces of impurities (from the materials synthesis for instance) which could segregate from the bulk of the oxide to the outer surface during the high temperature anneal. This demonstrates the difficulty of measuring the “intrinsic” surface exchange coefficient of these complex oxide materials. The observed interplay between segregation, decomposition and reorganization of the surface and subsurface layers and their complex evolution with time and temperature, coupled with the probable sensitivity to the ambient gas phase composition makes inter-comparison of experimental values of the surface exchange coefficient difficult.

AUTHOR INFORMATION

Corresponding Author

* Mónica Burriel, monica.burriel@grenoble-inp.fr, Univ. Grenoble Alpes, CNRS, LMGP, F-38000 Grenoble, France

Author Contributions

The manuscript was written through contributions of all authors. All authors have given approval to the final version of the manuscript.

ACKNOWLEDGMENT

Financial supports is acknowledged from the 7th European Community Framework Programme of the European Union (Marie Curie Intra European fellowship PIEF-GA-2009-252711 for M.B.), from wpi-IC2NER and from the Japanese Society for Promotion of Science (JSPS postdoctoral fellowship and Kakenhi Grant-in-Aid P13770 for H.T.). The authors also thank Dr. John Druce (Kyushu University) for assistance with LEIS measurements.

REFERENCES

- (1) Tarancón, A.; Burriel, M.; Santiso, J.; Skinner, S. J.; Kilner, J. A. Advances in Layered Oxide Cathodes for Intermediate Temperature Solid Oxide Fuel Cells. *J. Mater. Chem.* **2010**, *20* (19), 3799.
- (2) Boehm, E.; Bassat, J.; Dordor, P.; Mauvy, F.; Grenier, J.; Stevens, P. Oxygen Diffusion and Transport Properties in Non-Stoichiometric LnNiO Oxides. *Solid State Ionics* **2005**, *176* (37-38), 2717–2725.
- (3) Agudero, A.; Fawcett, L.; Taub, S.; Woolley, R.; Wu, K.-T.; Xu, N.; Kilner, J. A.; Skinner, S. J. Materials Development for Intermediate-Temperature Solid Oxide Electrochemical Devices. *J. Mater. Sci.* **2012**, *47* (9), 3925–3948.
- (4) Orera, A.; Slater, P. R. New Chemical Systems for Solid Oxide Fuel Cells †. *Chem. Mater.* **2010**, *22* (3), 675–690.
- (5) Jacobson, A. J. Materials for Solid Oxide Fuel Cells †. *Chem. Mater.* **2010**, *22* (3), 660–674.
- (6) Kilner, J. A.; Burriel, M. Materials for Intermediate-Temperature Solid-Oxide Fuel Cells. *Annu. Rev. Mater. Res.* **2014**, *44* (1), 365–393.

- (7) Sharma, R. K.; Burriel, M.; Dessemond, L.; Martin, V.; Bassat, J.-M.; Djurado, E. An Innovative Architectural Design to Enhance the Electrochemical Performance of $\text{La}_2\text{NiO}_{4+\delta}$ Cathodes for Solid Oxide Fuel Cell Applications. *J. Power Sources* **2016**, *316*, 17–28.
- (8) Ferchaud, C.; Grenier, J.-C.; Zhang-Steenwinkel, Y.; van Tuel, M. M. A.; van Berkel, F. P. F.; Bassat, J.-M. High Performance Praseodymium Nickelate Oxide Cathode for Low Temperature Solid Oxide Fuel Cell. *J. Power Sources* **2011**, *196* (4), 1872–1879.
- (9) Sayers, R.; De Souza, R. A.; Kilner, J. A.; Skinner, S. J. Low Temperature Diffusion and Oxygen Stoichiometry in Lanthanum Nickelate. *Solid State Ionics* **2010**, *181* (8-10), 386–391.
- (10) Skinner, S. J. Characterisation of $\text{La}_2\text{NiO}_{4+\delta}$ Using in-Situ High Temperature Neutron Powder Diffraction. *Solid State Sci.* **2003**, *5* (3), 419–426.
- (11) Nakamura, T.; Takeyama, Y.; Watanabe, S.; Yashiro, K.; Sato, K.; Hashida, T.; Mizusaki, J. Oxygen Nonstoichiometry, Crystal Structure and Mechanical Properties of $\text{La}_2\text{NiO}_{4+\delta}$. In *ECS Transactions*; ECS, 2009; pp 2573–2580.
- (12) Kharton, V. V.; Kovalevsky, A. V.; Avdeev, M.; Tsipis, E. V.; Patrakeevev, M. V.; Yaremchenko, A. A.; Naumovich, E. N.; Frade, J. R. Chemically Induced Expansion of $\text{La}_2\text{NiO}_{4+\delta}$ -Based Materials. *Chem. Mater.* **2007**, *19* (8), 2027–2033.
- (13) Bassat, J. M.; Odier, P.; Villesuzanne, A.; Marin, C.; Pouchard, M. Anisotropic Ionic Transport Properties in $\text{La}_2\text{NiO}_{4+\delta}$ Single Crystals. *Solid State Ionics* **2004**, *167* (3-4), 341–347.

- (14) Burriel, M.; Garcia, G.; Santiso, J.; Kilner, J. A.; Chater, R. J.; Skinner, S. J. Anisotropic Oxygen Diffusion Properties in Epitaxial Thin Films of $\text{La}_2\text{NiO}_{4+\delta}$. *J. Mater. Chem.* **2008**, *18* (4), 416.
- (15) Burriel, M.; Santiso, J.; Rossell, M. D.; Van Tendeloo, G.; Figueras, A.; Garcia, G. Enhancing Total Conductivity of $\text{La}_2\text{NiO}_{4+\delta}$ Epitaxial Thin Films by Reducing Thickness. *J. Phys. Chem. C* **2008**, *112* (29), 10982–10987.
- (16) Garcia, G.; Burriel, M.; Bonanos, N.; Santiso, J. Electrical Conductivity and Oxygen Exchange Kinetics of $\text{La}_2\text{NiO}_{4+\delta}$ Thin Films Grown by Chemical Vapor Deposition. *J. Electrochem. Soc.* **2008**, *155* (3), P28–P32.
- (17) Frayret, C.; Villesuzanne, A.; Pouchard, M. Application of Density Functional Theory to the Modeling of the Mixed Ionic and Electronic Conductor $\text{La}_2\text{NiO}_{4+\delta}$: Lattice Relaxation, Oxygen Mobility, and Energetics of Frenkel Defects. *Chem. Mater.* **2005**, *17* (26), 6538–6544.
- (18) Chroneos, A.; Parfitt, D.; Kilner, J. A.; Grimes, R. W. Anisotropic Oxygen Diffusion in Tetragonal $\text{La}_2\text{NiO}_{4+\delta}$: Molecular Dynamics Calculations. *J. Mater. Chem.* **2010**, *20* (2), 266.
- (19) Cleave, A. R.; Kilner, J. A.; Skinner, S. J.; Murphy, S. T.; Grimes, R. W. Atomistic Computer Simulation of Oxygen Ion Conduction Mechanisms in La_2NiO_4 . *Solid State Ionics* **2008**, *179* (21-26), 823–826.
- (20) Parfitt, D.; Chroneos, A.; Kilner, J. A.; Grimes, R. W. Molecular Dynamics Study of Oxygen Diffusion in $\text{Pr}_2\text{NiO}_{4+\delta}$. *Phys Chem Chem Phys* **2010**, *12* (25), 6834–6836.

- (21) Kuklja, M. M.; Kotomin, E. A.; Merkle, R.; Mastrikov, Y. A.; Maier, J. Combined Theoretical and Experimental Analysis of Processes Determining Cathode Performance in Solid Oxide Fuel Cells. *Phys. Chem. Chem. Phys.* **2013**, *15* (15), 5443–5471.
- (22) Bassat, J.-M.; Burriel, M.; Wahyudi, O.; Castaing, R.; Ceretti, M.; Veber, P.; Weill, I.; Villesuzanne, A.; Grenier, J.-C.; Paulus, W.; et al. Anisotropic Oxygen Diffusion Properties in Pr₂NiO_{4+δ} and Nd₂NiO_{4+δ} Single Crystals. *J. Phys. Chem. C* **2013**, *117* (50), 26466–26472.
- (23) Ananyev, M. V.; Tropin, E. S.; Eremin, V. A.; Farlenkov, A. S.; Smirnov, A. S.; Kolchugin, A. A.; Porotnikova, N. M.; Khodimchuk, A. V.; Berenov, A. V.; Kurumchin, E. K. Oxygen Isotope Exchange in La₂NiO_{4+δ}. *Phys. Chem. Chem. Phys.* **2016**, *18* (13), 9102–9111.
- (24) Hildenbrand, N.; Nammensma, P.; Blank, D. H. A.; Bouwmeester, H. J. M.; Boukamp, B. A. Influence of Configuration and Microstructure on Performance of La₂NiO_{4+δ} Intermediate-Temperature Solid Oxide Fuel Cells Cathodes. *J. Power Sources* **2013**, *238*, 442–453.
- (25) Burriel, M.; Wilkins, S.; Hill, J. P.; Munoz-Marquez, M. A.; Brongersma, H. H.; Kilner, J. A.; Ryan, M. P.; Skinner, S. J. Absence of Ni on the Outer Surface of Sr Doped La₂NiO₄ Single Crystals. *Energy Environ. Sci.* **2014**, *7* (1), 311–316.
- (26) Chen, Y.; Téllez, H.; Burriel, M.; Yang, F.; Tsvetkov, N.; Cai, Z.; McComb, D. W.; Kilner, J. A.; Yildiz, B. Segregated Chemistry and Structure on (001) and (100) Surfaces of (La_{1–X}Sr_X)₂CoO₄ Override the Crystal Anisotropy in Oxygen Exchange Kinetics. *Chem. Mater.* **2015**, *27* (15), 5436–5450.

(27) Wu, K.-T.; Tellez, H.; Druce, J.; Burriel, M.; Ishihara, T.; Kilner, J. A.; Skinner, S. J. Surface Composition of Layered Ruddlesden-Popper $\text{La}_{n+1}\text{Ni}_n\text{O}_{3n+1}$ ($n = 1, 2$ and 3) Epitaxial Films. *ECS Trans.* **2015**, *66* (2), 89–93.

(28) Druce, J.; Téllez, H.; Burriel, M.; Sharp, M. D.; Fawcett, L. J.; Cook, S. N.; McPhail, D. S.; Ishihara, T.; Brongersma, H. H.; Kilner, J. A. Surface Termination and Subsurface Restructuring of Perovskite-Based Solid Oxide Electrode Materials. *Energy Environ. Sci.* **2014**, *7* (11), 3593–3599.

(29) Druce, J.; Ishihara, T.; Kilner, J. Surface Composition of Perovskite-Type Materials Studied by Low Energy Ion Scattering (LEIS). *Solid State Ionics* **2014**, *262*, 893–896.

(30) Téllez, H.; Druce, J.; Ju, Y.-W.; Kilner, J.; Ishihara, T. Surface Chemistry Evolution in $\text{LnBaCo}_2\text{O}_{5+\delta}$ Double Perovskites for Oxygen Electrodes. *Int. J. Hydrogen Energy* **2014**, *39* (35), 20856–20863.

(31) Téllez, H.; Druce, J.; Kilner, J. a; Ishihara, T. Relating Surface Chemistry and Oxygen Surface Exchange in $\text{LnBaCo}_2\text{O}_{5-\delta}$ Air Electrodes. *Faraday Discuss.* **2015**.

(32) Druce, J.; Tellez, H.; Ishihara, T.; Kilner, J. A. Surface Segregation in Solid Oxide Electrode Materials Occurring at Intermediate Temperatures. *ECS Trans.* **2015**, *66* (2), 61–68.

(33) Wu, J.; Pramana, S. S.; Skinner, S. J.; Kilner, J. a; Horsfield, A. Why Ni Is Absent from the Surface of $\text{La}_2\text{NiO}_{4+\delta}$. *J. Mater. Chem. A* **2015**.

(34) Brongersma, H. H.; Grehl, T.; van Hal, P. A.; Kuijpers, N. C. W.; Mathijssen, S. G. J.; Schofield, E. R.; Smith, R. A. P.; ter Veen, H. R. J. High-Sensitivity and High-Resolution Low-Energy Ion Scattering. *Vacuum* **2010**, *84* (8), 1005–1007.

- (35) Brongersma, H.; Draxler, M.; Deridder, M.; Bauer, P. Surface Composition Analysis by Low-Energy Ion Scattering. *Surf. Sci. Rep.* **2007**, *62* (3), 63–109.
- (36) Brongersma, H. H. Low-Energy Ion Scattering. In *Characterization of Materials*; Kaufmann, E. N., Ed.; John Wiley & Sons, Inc.: Hoboken, NJ, USA, 2012; pp 2024–2044.
- (37) Tranquada, J. M.; Kong, Y.; Lorenzo, J. E.; Buttrey, D. J.; Rice, D. E.; Sachan, V. Oxygen Intercalation, Stage Ordering, and Phase Separation in $\text{La}_2\text{NiO}_{4+\delta}$ with $0.05 \leq \delta \leq 0.11$. *Phys. Rev. B* **1994**, *50* (9), 6340–6351.
- (38) Ouladdiaf, B.; Archer, J.; McIntyre, G. J.; Hewat, A. W.; Brau, D.; York, S. OrientExpress: A New System for Laue Neutron Diffraction. *Phys. B Condens. Matter* **2006**, *385-386*, 1052–1054.
- (39) Kilner, J.; Steele, B.; Ilkov, L. Oxygen Self-Diffusion Studies Using Negative-Ion Secondary Ion Mass Spectrometry (SIMS). *Solid State Ionics* **1984**, *12* (1984), 89–97.
- (40) DE SOUZA, R.; ZEHNPENNING, J.; MARTIN, M.; MAIER, J. Determining Oxygen Isotope Profiles in Oxides with Time-of-Flight SIMS. *Solid State Ionics* **2005**, *176* (15-16), 1465–1471.
- (41) Ziegler, J. F.; Biersack, J. P.; Littmark, U. *The Stopping and Range of Ions in Solids*; Pergamon, 1985.
- (42) Crank, J. *The Mathematics of Diffusion*; Clarendon Press, 1979.
- (43) Skinner, S. J.; Kilner, J. A. Oxygen Diffusion and Surface Exchange in $\text{La}_{2-x}\text{Sr}_x\text{NiO}_{4+\delta}$. *Solid State Ionics* **2000**, *135* (1-4), 709–712.

(44) Lee, J. H.; Luo, G.; Tung, I. C.; Chang, S. H.; Luo, Z.; Malshe, M.; Gadre, M.; Bhattacharya, A.; Nakhmanson, S. M.; Eastman, J. A.; et al. Dynamic Layer Rearrangement during Growth of Layered Oxide Films by Molecular Beam Epitaxy. *Nat. Mater.* **2014**, *13* (9), 879–883.

(45) Gauquelin, N.; Weirich, T. E.; Ceretti, M.; Paulus, W.; Schroeder, M. Long-Term Structural Surface Modifications of Mixed Conducting $\text{La}_2\text{NiO}_{4+\delta}$ at High Temperatures. *Monatshefte für Chemie - Chem. Mon.* **2009**, *140* (9), 1095–1102.

(46) De Souza, R.; Chater, R. Oxygen Exchange and Diffusion Measurements: The Importance of Extracting the Correct Initial and Boundary Conditions. *Solid State Ionics* **2005**, *176* (23-24), 1915–1920.

(47) Ridder, M. De; Vervoort, A. G. J.; Welzenis, R. G. Van; Brongersma, H. H. The Limiting Factor for Oxygen Exchange at the Surface of Fuel Cell Electrolytes. **2003**, *156*, 255–262.

(48) Druce, J.; Téllez, H.; Hyodo, J. Surface Segregation and Poisoning in Materials for Low-Temperature SOFCs. *MRS Bull.* **2014**, *39* (09), 810–815.

(49) Ridder, M. De; Welzenis, R. G. Van; Brongersma, H. H.; Kreissig, U. Oxygen Exchange and Diffusion in the near Surface of Pure and Modified Yttria-Stabilised Zirconia. **2003**, *158*, 67–77.

Insert Table of Contents Graphic and Synopsis Here